Published online March 26, 2004

1886–1893 *Nucleic Acids Research, 2004, Vol. 32, No. 6*
DOI: 10.1093/nar/gkh343

Structural and functional analysis of Mre11-3

L. Matthew Arthur, Karin Gustausson[1], Karl-Peter Hopfner[2], Christian T. Carson[3], Travis H. Stracker[3], Annette Karcher[2], Diana Felton[4], Matthew D. Weitzman[3], John Tainer[1,4] and James P. Carney*

Radiation Oncology Research Laboratory, Department of Radiation Oncology, Molecular and Cell Biology Graduate Program and Greenebaum Cancer Center, University of Maryland School of Medicine, Baltimore, MD 21201, USA, [1]Department of Molecular Biology and Skaggs Institute for Chemical Biology, The Scripps Research Institute and [3]Laboratory of Genetics, Salk Institute for Biological Studies, La Jolla, CA 92037, USA, [2]Gene Center and Institute of Biochemistry, University of Munich, Munich, Germany and [4]Life Sciences Division, Lawrence Berkeley National Laboratory, Berkeley, CA 94720, USA

Received December 23, 2003; Revised and Accepted February 27, 2004

ABSTRACT

The Mre11, Rad50 and Nbs1 proteins make up the conserved multi-functional Mre11 (MRN) complex involved in multiple, critical DNA metabolic processes including double-strand break repair and telomere maintenance. The Mre11 protein is a nuclease with broad substrate recognition, but MRN-dependent processes requiring the nuclease activity are not clearly defined. Here, we report the functional and structural characterization of a nuclease-deficient Mre11 protein termed mre11-3. Importantly, the hmre11-3 protein has wild-type ability to bind DNA, Rad50 and Nbs1; however, nuclease activity was completely abrogated. When expressed in cell lines from patients with ataxia telangiectasia-like disorder (ATLD), hmre11-3 restored the formation of ionizing radiation-induced foci. Consistent with the biochemical results, the 2.3 Å crystal structure of mre11-3 from *Pyrococcus furiosus* revealed an active site structure with a wild-type-like metal-binding environment. The structural analysis of the H85L mutation provides a detailed molecular basis for the ability of mre11-3 to bind but not hydrolyze DNA. Together, these results establish that the mre11-3 protein provides an excellent system for dissecting nuclease-dependent and independent functions of the Mre11 complex.

INTRODUCTION

Cells have evolved many processes for repairing double-strand breaks (DSBs) in DNA. In mammals, repair of these breaks is essential to maintaining genomic integrity and preventing cancer. DSBs are induced by a variety of external [e.g. ionizing radiation (IR)] or internal (e.g. replication) agents and are repaired by two major pathways of recombination. One pathway is homologous recombination, which uses a sister chromatid or homologous chromosome as a template for DNA synthesis and rejoining. An alternative pathway of recombination is termed non-homologous end joining (NHEJ), in which two ends of the break are held in close proximity and ligated back together, frequently causing deletion or addition of nucleotides (1). Although these are distinct pathways, one protein complex that may play a role in both homologous recombination and NHEJ is the Mre11 complex.

Mre11 is found in complex with Rad50 that is conserved throughout all kingdoms of life. In eukaryotes, Mre11 and Rad50 interact with a third protein, Nbs1 (Xrs2 in yeast), that links the complex to DNA damage-induced cell cycle checkpoints (2,3). The yeast Mre11 complex has been implicated in a number of mitotic and meiotic pathways, telomere silencing and homologous recombination (4). In humans, mutations in hMre11 and Nbs1 are responsible for the chromosomal breakage syndromes ataxia telangiectasia-like disorder (ATLD) and Nijmegen breakage syndrome (NBS), respectively (3,5). Null mutations in higher organisms are embryonic lethal, while in yeast the mre11Δ mutant is highly sensitive to DNA-damaging agents that require recombinational repair (6–8). These phenotypes establish the importance of the complex in a number of DNA metabolic pathways.

Mre11 is evolutionarily conserved, particularly in the N-terminal region, which contains five phosphoesterase motifs that form the nuclease domain of the protein [see Fig. 1A; (9)]. The crystal structure of the nuclease domain from *Pyrococcus furiosus* Mre11 reveals that the phosphoesterase domains form the active site. Two metal ions are coordinated by five conserved phosphodiesterase motifs of the protein. The structure suggests that multiple nuclease activities are the result of a single endo/exonuclease mechanism which is controlled by access of DNA to the active site metals (10). In

*To whom correspondence should be addressed. Tel: +1 410 706 4276; Fax: +1 410 706 6138; Email: jcarney@som.umaryland.edu
Present address:
Travis H. Stracker, Memorial Sloan Kettering Cancer Center, New York, NY 10021, USA

The authors wish it to be known that, in their opinion, the first two authors should be regarded as joint First Authors

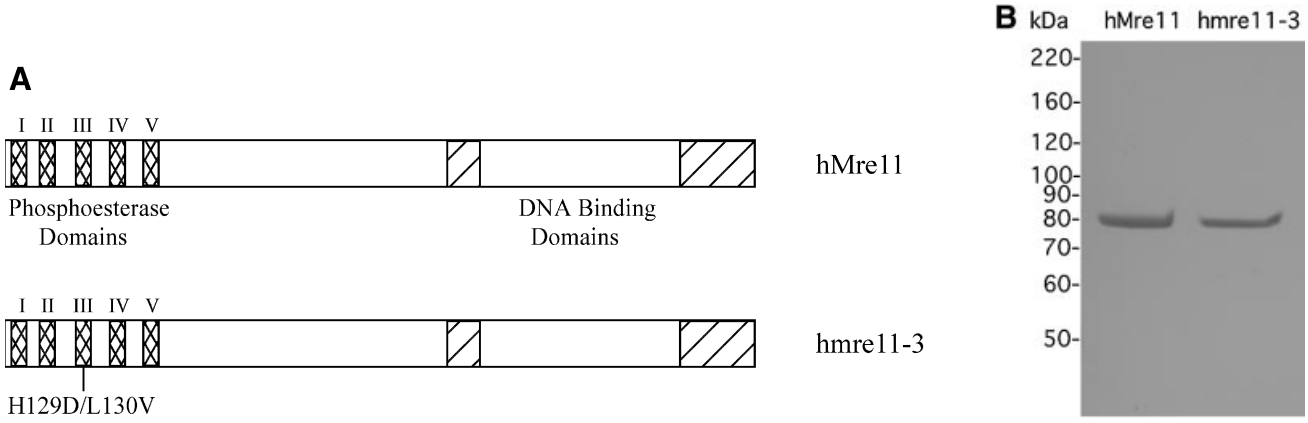

Figure 1. Schematic sequence and purity of wild-type and hmre11-3 mutant Mre11 proteins. (**A**) The N-terminus of Mre11 is evolutionarily conserved, specifically the five phosphoesterase domains (cross-hatch). The C-terminal domain contains two putative DNA-binding domains (diagonal hatch). The hmre11-3 protein has a mutation in the third phosphoesterase domain, specifically a histidine and aspartic acid at position 129 and 130 were converted to a leucine and valine, respectively. (**B**) Purified hMre11 (WT) and hmre11-3 analyzed by SDS–PAGE and Coomassie blue staining (left panel) and western blot (right panel).

the presence of Mn^{2+}, the active site of the protein binds to a dAMP molecule mainly through Asn84, His85 and two Mn^{2+} ions. Mechanistically, the crystal structure suggests that the His85 residue donates a proton to the leaving 3′-OH to complete the cleavage of the phosphate backbone (10). In *Saccharomyces cerevisiae*, mutations of conserved residues in the phosphoesterase domains increased sensitivity to IR and showed defects in DSB repair (11).

The role of the Mre11 nuclease in DSB repair is unclear; however, *in vitro* biochemical studies reveal three Mn^{2+}-dependent enzymatic activities: a single-stranded endonuclease, a double-stranded exonuclease and DNA hairpin opening (12–16). The Mre11 nuclease has been implicated in the suppression of CAG-mediated inhibition of DSB repair and the repair of inverted repeat-induced mitotic DSBs (17,18). These types of lesions cause hairpin structures at the site of the DSB that is one of the substrates of the Mre11 nuclease. In addition, the nuclease has been implicated in altering the gene conversion tract length in double-strand gap repair (19). These results might account for the marginal sensitivity to IR observed in scmre11-3 cells (11).

In this study, we investigated the structure and biochemical properties of the mutant mre11-3 protein. *In vitro* biochemical analysis showed that the hmre11-3 mutation completely abrogated the exonuclease activity. We also provide evidence that the ability to bind DNA in the presence of Mg^{2+}, which significantly reduces the nuclease activity, was similar to that of the wild-type protein. Protein interaction studies *in vitro* showed that the hmre11-3 mutation did not affect binding to human Rad50 or Nbs1. Additionally, we show that in ATLD cells complemented with hmre11-3, the complex can localize to DSBs in IR-induced foci (IRIF). To investigate further the effect of this mutation, the equivalent mutation was produced for the *P.furiosus* (pfmre11-3) protein. We furthermore report here that the crystal structure of pfmre11-3 has the same secondary and tertiary structure as the wild-type protein, with only small changes in the active site geometry. The structure is consistent with fairly normal DNA binding of pfmre11-3 and suggests that defects in nuclease activity result mainly from disturbed transition state chemistry. These findings suggest that the mre11-3 protein provides a powerful system for studying the role of the nuclease in human cells while maintaining the structural integrity of the complex.

MATERIALS AND METHODS

Expression and purification of proteins

Recombinant baculoviruses for hMre11, and mre11-3 were generated using the Bac to Bac system from Invitrogen as per the manufacturer's instructions. Two hundred ml cultures of Sf9 cells (1.00×10^6 cells/ml) were infected at an m.o.i. of approximately 10, and expression continued for 48 h. The cells were harvested and resuspended in 20 ml of buffer A (50 mM $NaPO_4$ pH 7.0, 500 mM NaCl, 20 mM β-mercaptoethanol, 20 mM imidazole and 5% glycerol). Cells were lysed by one freeze–thaw cycle and passage through a 25-gauge needle, then they were centrifuged at 100 000 *g* for 1 h at 4°C. Crude extract was applied to a HiTrap chelating column (Amersham/Pharmacia) that was equilibrated with 0.1 M $NiSO_4$, and protein was eluted on a 15 ml gradient in buffer A from 20 to 200 mM imidazole. Eluted protein was further purified by gel filtration chromatography on a Superdex 200 column (Amersham/Pharmacia) in buffer containing 50 mM Tris–HCl pH 8.0, 1 mM dithiothreitol (DTT) and 150 mM NaCl. SDS–PAGE and Coomassie blue staining were used to identify fractions containing hMre11 or mre11-3. The pooled gel filtration fractions were directly applied to a Resource Q column (Amersham/Pharmacia) and pre-equilibrated in a buffer containing 50 mM Tris–HCl pH 8.0, 1 mM DTT, 5% (w/v) glycerol and 50 mM NaCl. Proteins were eluted with a 10 ml gradient from 50 to 500 mM NaCl. Fractions containing hMre11 and the mutants were frozen in liquid nitrogen and stored at –80°C.

Exonuclease assays

Reactions contained 25 mM MOPS [3-(*N*-morpholino)propanesulfonic acid] pH 7.0, 60 mM KCl, 2 mM DTT and 5 mM

$MnCl_2$. Two separate exonuclease assays were performed to test for activity. The first assay was performed in 10 µl reactions using 2 pmol of protein with 0.3 pmol of ^{32}P-labeled single-stranded 40mer oligonucleotide annealed to an unlabeled complementary strand. The reactions were terminated by the addition of stop solution [0.05% (w/v) bromophenol blue, 0.05% (w/v) xylene cyanol and 2 mM EDTA prepared in deionized formamide]. Samples were boiled for 5 min, placed directly on ice, and loaded onto a 10% acrylamide/10% (w/v) formamide/7 M urea gel in 1× TBE. Gels were run for 1.5 h at 65 W, exposed to a phosphoimager screen for at least 4 h, and analyzed on a BioRad Personal FX Phosphoimager. We also performed additional exonuclease assays using 25 nM protein with 2.5 mM of single-stranded 40mer oligonucleotide, containing a 2-amino purine on the 3′ end, which was annealed to an unlabeled complementary strand. The release of 2-amino purine was measured by the absorption at 310 nM and emission at 375 nM determined by a spectrophotometer.

DNA gel shift assay

DNA gel shift assays were performed in 20 µl reactions containing 20 mM Tris–HCl pH 7.5, 80 mM NaCl, 1 mM DTT, 3% (v/w) glycerol, 5 mM $MgCl_2$, 0.4 mg/ml acetylated bovine serum albumin (BSA), 40 fmol ^{32}P-labeled single-stranded 40mer oligonucleotide, and various concentrations of proteins as indicated. Reactions were incubated for 15 min at room temperature before adding 2 µl of 50% glycerol to each reaction. Samples were loaded onto a 6% polyacrylamide gel and run at 250 V for 2 h in 0.5× Tris-borate buffer. Gels were then exposed to a phosphoimager screen for detection and analysis.

Cell, IR treatment and immunofluorescence

ATLD1 cells were a gift from J. Petrini and were immortalized by transduction with retroviruses expressing SV40 T-antigen and hTERT. These cells were then transduced with retroviruses expressing wild-type Mre11 or the mre11-3 mutant (20). Puromycin-resistant pools were selected and maintained at 1 µg/ml. All cells were maintained as monolayers in Dulbecco's modified Eagle's medium (DMEM) supplemented with 20% fetal bovine serum (FBS), at 37°C in a humidified atmosphere containing 5% CO_2. For immunofluorescence, cells were grown on glass coverslips in 24-well dishes and exposed to 10 Gy IR using a cobalt^{60} irradiation chamber. After 2 h, cells were fixed with a 1:1 mixture of MeOH and acetone, and immunofluorescence was performed with a primary antibody to Mre11 (Oncogene) and a fluorescein isothiocyanate (FITC)-labeled secondary antibody (Jackson Laboratories). Nuclear DNA was stained with 4′,6-diamidino-2-phenylindole (DAPI) and coverslips were mounted using Fluoromount-G (Southern Biotechnology Associates). Immunoreactivity was visualized using a Nikon microscope in conjunction with a CCD camera (Cooke Sensicam). Images were obtained in double or triple excitation mode and processed using SlideBook and Adobe Photoshop.

Crystallization, crystallographic data collection, MAD phasing and structure refinement of pfmre11-3

The pfmre11-H85L protein (12 mg/ml in 20 mM phosphate pH 7.5, 200 mM NaCl, 0.1 mM EDTA, 5% glycerol) was crystallized in space group $P2_12_12_1$ with cell dimensions a = 72.9, b = 87.0, c = 146.4 Å and two molecules in the asymmetric unit by sitting drop vapor diffusion at 4°C after mixing 2 µl of protein solution with 1.5 µl of precipitant solution (100 mM CHES pH 9.5, 400 mM ammonium sulfate, 35% PEG 600) as described (10). A data set to 2.3 Å resolution was recorded at beamlime 9-1 at SSRL (Stanford) using a Quantum 2 × 2 CCD detector. The data were processed with the HKL suite and reduced with TRUNCATE. As the start model, we used coordinates of wt-pfmre11 (PDB access 1II7), which crystallized in similar cell dimensions and space group. The start model could be directly positioned by rigid body minimization, treating both molecules in the asymmetric unit independently. After overall anisotropic B-value and bulk solvent correction, the structure was refined to 2.3 Å by cycles of positional and individual B-value refinement and manual model building with CNS (21) and MAIN (Table 1). Five percent of the data were excluded from refinement to calculate the free R-value for cross-validation. The models were rebuilt

Table 1. Crystallographic data collection and model refinement

Crystal data	
Space group	$P2_12_12_1$ (two molecules/asymmetric unit)
Unit cell dimensions (Å)	a = 75.0, b = 88.6, c = 145.0
Data collection	
Wavelength (Å)	1.080
Data range (Å)	30.0–2.3
Observations (unique)	352 858 (42 681)
Completeness (%) (last shell)	94.2 (94.1)
R_{sym}[a] (last shell)	0.041 (0.380)
$I/\sigma(I)$ (last shell)	16.3 (2.8)
Refinement	
Resolution range (Å)	30.0–2.3
Reflections $F>0$ (cross-validation)	40 877 (2044)
Non-hydrogen atoms (solvent molecules)	5864 (345)
R_{cryst}[b] (R_{free}[c])	0.225 (0.274)
R.m.s bond length (Å)/bond angles (°)	0.008 (1.45)
%core (disallowed) in Ramachandran plot	87.0 (0.0)

[a]R_{sym} is the unweighted R-value on I between symmetry mates.
[b]$R_{cryst} = \sum hkl||F_{obs}(hkl)| - |F_{calc}(hkl)||/\sum hkl|F_{obs}(hkl)|$.
[c]R_{free} = the cross validation R-factor for 5% of reflections against which the model was not refined.

with MAIN and refined with CNS. Refinement and model statistics are shown in Table 1.

RESULTS

Production and purification of hMre11 and hmre11-3

In order to examine the biochemical effects of the mre11-3 mutation, we expressed the wild-type (hMre11) and mutant protein (hmre11-3; H129L/D130V) in insect cells using a baculovirus expression system and purified to >95% homogeneity as determined by Coomassie blue staining (Fig. 1B). During the purification process, hmre11-3 eluted from both an anion exchange column (MonoQ) and a gel filtration column (Superdex200) in an identical fashion to the wild-type hMre11, suggesting that the mutation does not grossly alter the structure of hMre11 (data not shown).

hmre11-3 is deficient in nuclease activity

In order to examine the effect of the mre11-3 mutation on the catalytic activity of hMre11, we performed exonuclease assays on the hmre11-3 protein. A time course experiment was performed using a ^{32}P-labeled single-stranded 40mer oligonucleotide annealed to an unlabeled complementary strand. The individual reaction products were separated on a denaturing polyacrylamide gel and analyzed by phosphoimager. The hmre11-3 protein had no residual nuclease activity at five times the concentration of the wild-type protein (Fig. 2A). We also confirmed that the hmre11-3 protein was completely defective in exonuclease activity by measuring the release of a 2-amino purine base analog at the 3′-penultimate position of an oligonucleotide substrate by fluorescence spectroscopy (Fig. 2B). These results indicate that the conserved His129 residue is required for nuclease activity of hMre11.

DNA binding capability of the hmre11-3 protein

Based on the *P.furiosus* Mre11 crystal structure, the conserved histidine residue in the third phosphoesterase domain is involved in binding of a dAMP molecule, which is the product of the nuclease reaction (10). If the His85 residue of *P.furiosus* acts in transition state stabilization during cleavage, the initial DNA binding of the reaction would not be affected. In order to test this, we examined the ability of the hmre11-3 protein to bind DNA in the presence of Mg^{2+}, which significantly reduces the Mn^{2+}-dependent nuclease activity of Mre11 and allows for DNA binding activity to be assessed. We performed gel retardation assays with the wild-type and hmre11-3 proteins. The mutant protein was able to bind to the DNA at levels comparable with the wild-type protein (Fig. 3). However, we routinely observe two protein:DNA complexes in the gel shift experiments, and the relative ratio of these two complexes is altered with hmre11-3 bound. These results validate the crystal structure prediction that the His85 residue in *P.furiosus* is involved in exonuclease activity but not in the initial binding of DNA.

Rad50 and Nbs1 are able to interact with hmre11-3

Mre11 acts in a DNA DSB repair complex with Rad50 and Nbs1 in humans (9). To examine the interaction capabilities using the human proteins, we co-expressed a His-tagged hMre11 or hmre11-3 protein with an untagged hRad50

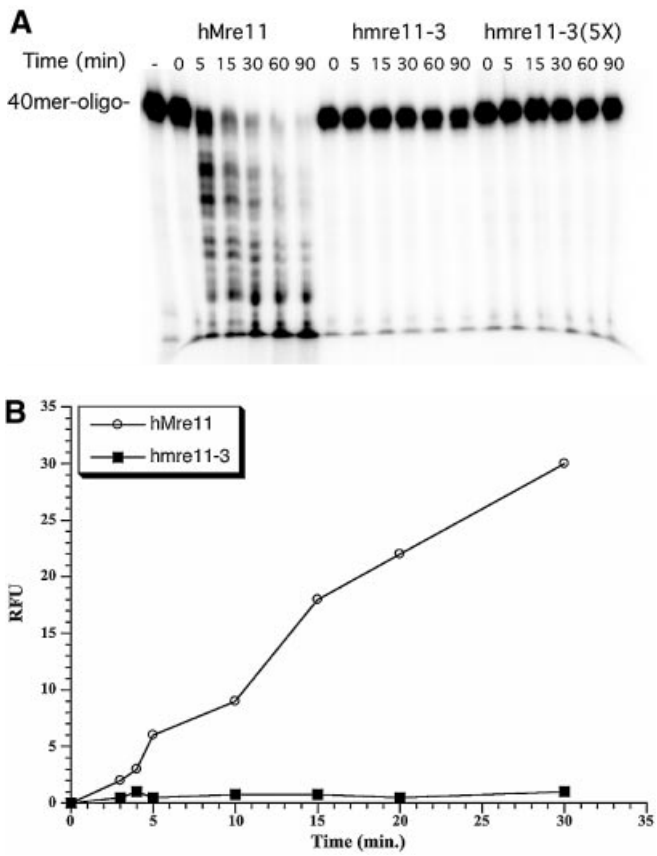

Figure 2. Exonuclease activities of the hmre11-3 mutant protein. (**A**) Proteins were tested for activity on a double-stranded 40mer oligonucleotide as described in Materials and Methods. Aliquots were removed from the reactions at the indicated time points, and at the conclusion of the reaction (90 min) the reaction products were separated on a denaturing acrylamide gel and visualized by phosphoimager. The mre11-3 protein showed no activity at five times the concentration of wild type. (**B**) Exonuclease assays were also performed using 25 nM protein with 2.5 mM of 10mer double-stranded oligo containing a single 2-amino purine that is six bases from the 3′ end. The release of the 2-amino purine over a time course was measured on a spectrophotometer.

protein. Crude samples were applied to an Ni^{2+}-NTA column and eluted with imidazole. Protein interaction was analyzed by western blot of the elutions with Rad50 and Mre11 antiserum, and the interactions of Rad50 and hmre11-3 were equivalent to that of Rad50 with hMre11 (Fig. 4A). We also examined the interaction with the Nbs1 protein using co-infections of His-tagged Nbs1 with hMre11 or hmre11-3. After purification by Ni^{2+}-NTA affinity chromatography, we carried out gel filtration chromatography. Following separation of the respective hMre11–Nbs1 complexes on a Superdex 200 column, we analyzed the fractions by SDS–PAGE and Coomassie blue staining. When expressed together, the hMre11 and Nbs1 proteins form a stable complex that elutes at a size of ~470 kDa while the Nbs1 protein elutes at ~200 kDa, and hMre11 alone elutes at ~150 kDa (Fig. 4B). Gel filtration chromatography of the hmre11-3 protein with Nbs1 reveals that this complex elutes at a position identical to the hMre11 and Nbs1 heterodimer (Fig. 4B), indicating that the hmre11-3 protein

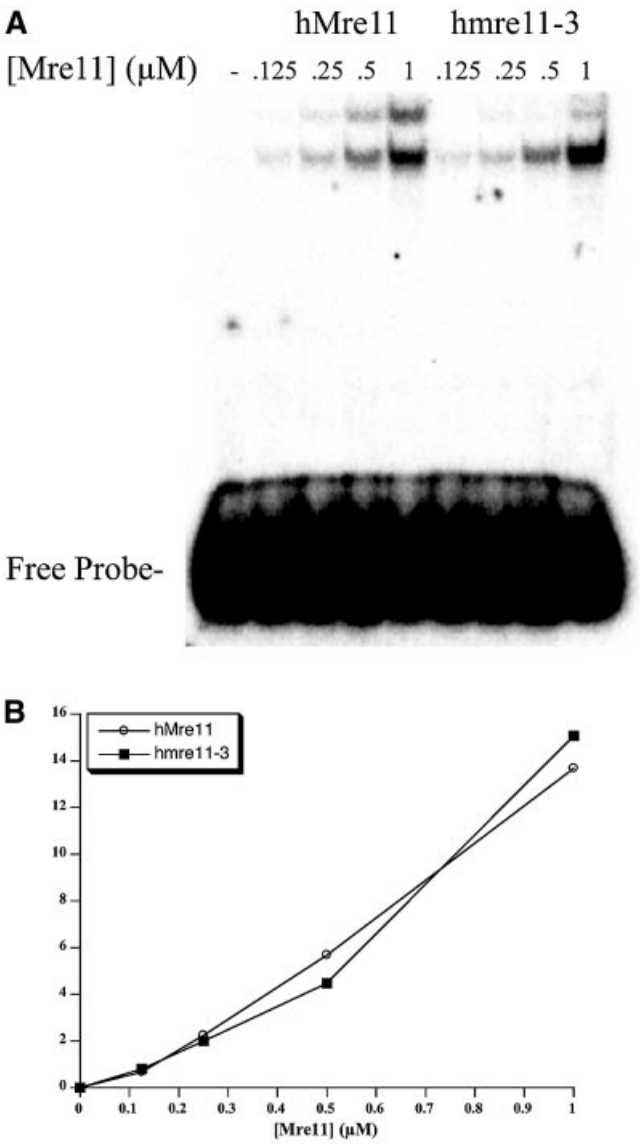

Figure 3. DNA binding tested by DNA gel shift assay. (**A**) DNA binding capabilities of hMre11 and hmre11-3 were assessed by gel shift assay using a single-stranded 40mer oligonucleotide as a probe. The probe was incubated with increasing protein concentrations (μM). Protein:DNA complexes were resolved on a native polyacrylamide gel and visualized by a phosphoimager. (**B**) The gel in (A) was quantitated and percent DNA shifted is plotted versus amount of protein added. No difference in binding was observed between hMre11 and hmre11-3.

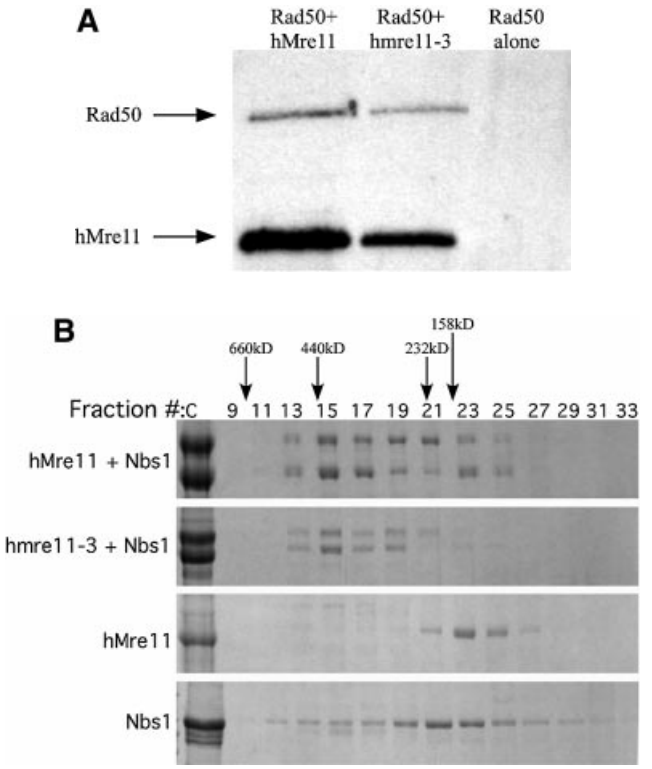

Figure 4. Preserved interactions in the Mre11 protein complex proteins. (**A**) Crude samples from co-infections of Sf9 cells using His-tagged hMre11 (lane 1) or hmre11-3 (lane 2) virus with an untagged Rad50, and Rad50 alone (lane 3) were applied to Ni-NTA beads and eluted using imidazole. Elutions were run on a polyacrylamide gel and a western blot was performed using Mre11 and Rad50 antibodies. (**B**) Fractions from a gel filtration column run on a polyacrylamide gel. Co-infections of Sf9 cells using His-tagged hMre11 or hmre11-3 virus with a His-tagged Nbs1 virus were purified on a nickel column. The samples were subsequently fractionated on a Superdex 200 column. The hMre11 (top panel) and hmre11-3 (second from top panel) proteins, co-expressed with Nbs1, demonstrate a shift from a lower molecular weight to a higher molecular weight when compared with hMre11 (second from bottom panel) or Nbs1 (bottom panel) alone.

forms a stable complex with Nbs1. IRIF are formed in ATLD cells complemented with hmre11-3

To test a functional interaction of the hmre11-3 protein with other members of the complex, we examined the accumulation of the Mre11 complex at foci in response to DSBs. Two patient cell lines (ATLD1 and ATLD3) were complemented with either wild-type hMre11 or the hmre11-3 mutant by retrovirus transduction. In ATLD1, there is a total loss of full-length hMre11 and only a truncated protein is expressed (5). In ATLD3, there are reduced levels of a partially active hMre11 with a missense mutation and the N117S amino acid change (5). In both cell lines, the levels of Rad50 and Nbs1 proteins are also reduced and are much more cytoplasmic than the predominantly nuclear localization observed in normal cells. Expression of both the wild-type and hmre11-3 proteins in either ATLD1 or ATLD3 cells led to stabilization of the Rad50 and Nbs1 proteins and their relocalization to the nucleus (22) (data not shown). We examined whether the Mre11 proteins accumulate at IRIF in complemented ATLD cell lines (Fig. 5). Immunofluorescence revealed foci of Mre11 in cell lines complemented with both wild-type and hmre11-3 mutant protein. These were observed in both ATLD1 and ATLD3 complemented cell lines (data not shown). Together these results demonstrate that the hmre11-3 mutant is capable of assembling into a partially functional complex with Rad50 and Nbs1 proteins in human cells.

Crystal structure of the pfmre11-3 protein

To experimentally define the effects of the mre11-3 mutation on the active site conformation of Mre11, we crystallized pfMre11-3 in the manganese-bound form and determined the crystal structure to 2.3 Å resolution. The active site of Mre11

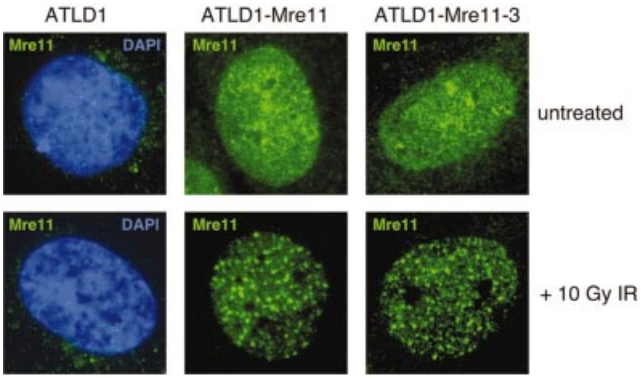

Figure 5. Mre11 complex foci formation in cells complemented with wild-type and hmre11-3 proteins. ATLD1 cells were complemented by transduction with retrovirus vector expressing wild-type hMre11 and the hmre11-3 mutant. Cells were untreated or were exposed to 10 Gy IR and allowed to recover for 2 h prior to immunofluorescence with an Mre11 antibody. In ATLD1 cells, faint staining for the truncated Mre11 protein was observed mainly in the cytoplasm (DAPI staining marks the nuclei). In complemented cells, the hMre11 and hmre11-3 proteins appear in the nucleus and both form foci upon IR treatment. Focus formation was analyzed in pools of transduced cells. In both cases, foci were observed in the majority of cells expressing detectable levels of the Mre11 protein in the nucleus. The appearance of the foci for wild-type hMre11 and mutant hmre11-3 was similar.

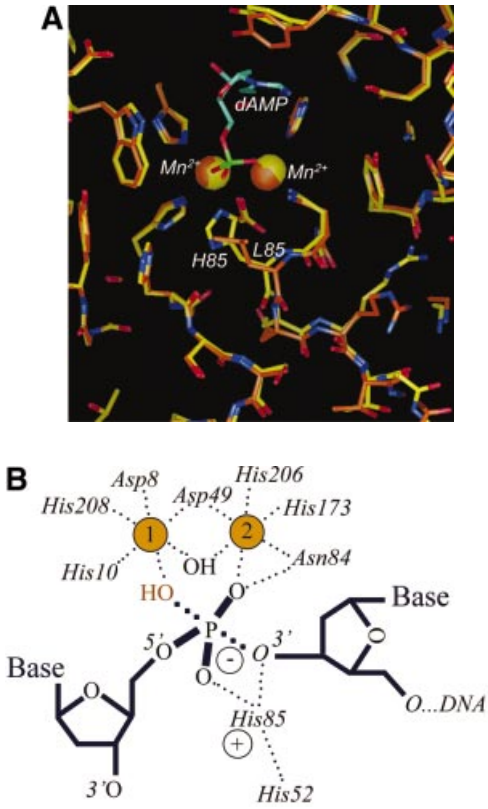

Figure 6. Crystal structure of pfMre11-3, active site preservation and implicated transition state alterations. (**A**) Superposition of the refined crystal structure of pfMre11-3 (tube model with orange carbons, red oxygen and blue nitrogen atoms) with the previously determined structure of manganese-dAMP-bound wild-type pfMre11 (tube model with yellow carbons, red oxygen and blue nitrogen atoms). The two active site manganese ions are shown as orange (Mre11-3) or yellow (wild-type) spheres. The dAMP molecule (wild-type) is shown in cyan. With the exception of the backbone loop at His85, the active sites of wild-type and mutated Mre11 are structurally conserved, including the position and coordination of the manganese ions. This structural conservation suggests that metal and substrate binding by Mre11 is mostly undisturbed, whereas transition state stabilization is implied to be defective, due to disruption of the conserved His52–His85 charge relay system. (**B**) Proposed structure and mechanism of transition state stabilization by Mre11 as deduced from wild-type and mutant Mre11 structure and biochemistry. The DNA backbone at the scissile bond is bound to one of two metals (yellow spheres), whereas the other metal activates a hydroxide ion for nucleophilic attack. In the expected pentacoordinated phosphate transition state, His85 evidently stabilizes the developing negative charge by binding to the unliganded phosphate oxygen and possibly also the leaving group oxygen.

contains two manganese ions that are critical for nucleolytic activity. Both ions are clearly visible in the structure of pfmre11-3, showing that pfmre11-3 is capable of efficiently coordinating manganese. Moreover, the crystal structure of mre11-3 revealed essentially the same overall fold and active site conformation as the previously determined wild-type Mre11 structure (Fig. 6). This suggests that the reduced nuclease activity is not due to a misfolded active site or loss or deformation of the metal-binding environment. In the immediate vicinity of His85Leu, two manganese ions were coordinated by His10, His173, His206, His208, Asp8 and Asp49, as well as Asn84 side chains, as has been observed for wild-type Mre11. However, the His85Leu mutation, which is located immediately adjacent to the metal-binding site, induces a backbone flexibility as judged by partially disordered electron density portions. This backbone flexibility at positions 85 and 86 probaby affects the neighboring Asn84 and could therefore influence the metal-binding properties of pfmre11-3 directly.

More importantly, His85 is positioned where it would be likely to bind the phosphate–sugar moiety at the scissile bond, since it was observed to coordinate the product state phosphate in the dAMP complex of Mre11 (10). Replacement of histidine with leucine therefore abolished a potential stabilization of the negatively charged, pentacoordinated phosphate transition state that occurs during backbone cleavage. Thus, the structural analysis suggests that nuclease defects of mre11-3 presumably arise from a reduced transition state stabilization and substrate orientation rather than a deformed metal-binding environment or abolished DNA binding activity.

DISCUSSION

The Mre11 complex acts in DNA repair, checkpoint signaling, homologous recombination and telomere maintenance (4,9,23). Previous crystal structure data of the *P.furiosus* Mre11 protein revealed a protein phosphatase-like, dimanganese-binding domain that is responsible for the endo/exonuclease function (10). The active site for Mre11 closely resembles the di-metal-binding motifs of the Ser/Thr phosphatases (24). To better understand the mechanism of nuclease activity of the Mre11 protein, we determined crystal structures of the *P.furiosus* mre11-3 catalytic domain. The comparison of the pfMre11 protein with pfmre11-3 revealed that the structure of the proteins is remarkably unchanged and that the defect in nuclease activity is not due to a conformational change. The dAMP bound to the active site of the Mre11

protein suggests that the mutation in the conserved histidine residue does not effect the binding to DNA, but instead is unable to form a charge relay to protonate the leaving 3′O to complete cleavage. This analysis could also explain our results that hmre11-3 protein has no defective DNA binding activity.

Our results indicate that there are no large structural differences in the metal-binding site and active site geometry of Mre11-3 and the wild-type Mre11 protein. The structural results indicate that the abolished nuclease activity of Mre11-3 does not stem from an abolished or largely altered interaction of Mre11 with DNA substrates, consistent with the biochemically observed DNA binding activity of Mre11-3. Rather, the specific stabilization of the DNA–protein transition state in phosphoesterolysis could be disturbed. The dAMP phosphate is coordinated by the two metals and by a bond to His85 εN. By comparison with the related protein tyrosine phosphatases, this coordination probably reflects the product state of the enzyme. In the ground and transition state, the DNA backbone phosphate is bound only to one metal. The other metal positions the attacking hydroxide ion that becomes the second coordinating oxygen in the product state (Fig. 6B). In the pentacoordinated transition state, the developing negative charge could be specifically stabilized by His85, which is positioned to bind to both the leaving group oxygen and a non-metal-bound oxygen of the phosphate (which is equivalent to the His85-binding oxygen of the dAMP–phosphate complex). Adjacent to His85 is the conserved His52 (second phosphoesterase motif). The location and sequence conservation suggest that His85 and His52 could form a charge relay system to stabilize the positive charge on His85. Our results thus confirm and extend the previous structure-based nuclease mechanism that relies on the conserved histidine residue in the third phosphoesterase domain for cleavage.

To help define the role of the Mre11 nuclease activity in the functions of the Mre11 complex, it is essential that mutant proteins are not defective for assembly into a protein complex with Rad50 and Nbs1. Previous two-hybrid studies in *S.cerevisiae* suggested that the (sc)mre11-3 and hmre11-3 proteins retained their interactions with Rad50 (11). We have now shown experimentally that the hmre11-3 mutant assembles a complex with Rad50 and Nbs1 proteins. Additionally, we show that the mutant protein accumulates in foci after exposure of complemented cells to IR that resemble the wild-type Mre11 complex response. This defined system will now allow tests of nuclease-dependent and -independent Mre11 complex functions. For example, it will be interesting to determine whether cells complemented with this mutant display normal signaling and checkpoint activation upon DNA damage. Another proposed role for the Mre11 nuclease is in processing of DSBs during meiosis where the Mre11 complex has been implicated in removal of the covalently bound Spo11 protein (4,25). The Mre11 nuclease has also been suggested to be involved in removing the adenoviral terminal protein that is covalently bound to the ends of the adenoviral genome (22). Removal of the terminal protein allows concatemerization of the adenoviral genomic DNA through the NHEJ pathway. In ATLD cells complemented with wild-type Mre11, viral concatemers are formed but these are not observed with the hmre11-3 mutant (22). Additionally, recent work has shown a requirement for the Mre11 complex in activation of the ATM protein kinase during the DNA damage response (26,27). As most of this work has been conducted in ATLD mutant cells, it will be important to determine whether the endogenous mutant proteins expressed in the ATLD cells are stabilized and recruited into the Mre11 complex when the hmre11-3 protein is expressed. Currently, our results establish the ability of the mre11-3 nuclease protein to assemble normal appearing Mre11 complexes and create normal appearing foci in response to IR. This system therefore provides a validated tool for studying the specific functions of the Mre11 nuclease while maintaining other functions of the Mre11 protein.

ACKNOWLEDGEMENTS

We are grateful to T. Paull for the Mre11 cDNA and J. Petrini for ATLD cells. We thank J. Karlseder and C. Lilley for help with immortalization and complementation of ATLD cells. We acknowledge the James B. Pendelton Charitable Trust for providing the Pendelton Microscopy Facility at the Salk Institute. This work was supported in part by NIH grants CA87851 (J.P.C.), CA92584 (J.P.C. and J.A.T.), AI43341 and CA97093 (M.D.W.), and American Cancer Society grant RPG0005901CCE (J.P.C.). K.P.H. and K.G. were supported in part by Fellowships from the Skaggs Institute for Chemical Biology. L.M.A. was supported by a Dissertation Fellowship from the Susan G. Komen Foundation, and C.T.C. was supported by the Timken-Sturgis Foundation and by an NIH Training Grant to the Salk Institute. T.H.S. was supported by fellowships from the H.A. and Mary K. Chapman Charitable Trust, the Legler Benbough Foundation and the Salk Institute Association. Coordinates have been deposited with the RCSB Protein Data Bank with accession code 1S8E.

REFERENCES

1. Critchlow,S.E. and Jackson,S.P. (1998) DNA end-joining: from yeast to man. *Trends Biochem. Sci.*, **23**, 394–398.
2. Varon,R., Vissinga,C., Platzer,M., Cerosaletti,K.M., Chrzanowska,K.H., Saar,K., Beckmann,G., Seemanova,E., Cooper,P.R., Nowak,N.J. *et al.* (1998) Nibrin, a novel DNA double-strand break repair protein, is mutated in Nijmegen breakage syndrome. *Cell*, **93**, 467–476.
3. Carney,J.P., Maser,R.S., Olivares,H., Davis,E.M., Le Beau,M., Yates,J.R., 3rd, Hays,L., Morgan,W.F. and Petrini,J.H. (1998) The hMre11/hRad50 protein complex and Nijmegen breakage syndrome: linkage of double-strand break repair to the cellular DNA damage response. *Cell*, **93**, 477–486.
4. Haber,J.E. (1998) The many interfaces of Mre11. *Cell*, **95**, 583–586.
5. Stewart,G.S., Maser,R.S., Stankovic,T., Bressan,D.A., Kaplan,M.I., Jaspers,N.G., Raams,A., Byrd,P.J., Petrini,J.H. and Taylor,A.M. (1999) The DNA double-strand break repair gene hMRE11 is mutated in individuals with an ataxia-telangiectasia-like disorder. *Cell*, **99**, 577–587.
6. Johzuka,K. and Ogawa,H. (1995) Interaction of Mre11 and Rad50: two proteins required for DNA repair and meiosis-specific double-strand break formation in *Saccharamoyces cerevisiae*. *Genetics*, **139**, 1521–1532.
7. Nairz,K. and Klein,F. (1997) mre11S—a yeast mutation that blocks double-strand-break processing and permits nonhomologous synapsis in meiosis. *Genes Dev.*, **11**, 2272–2290.
8. Chamankhah,M. and Xiao,W. (1998) Molecular cloning and genetic characterization of the *Saccharomyces cerevisiae* NGS1/MRE11 gene. *Curr. Genet.*, **34**, 368–374.
9. D'Amours,D. and Jackson,S.P. (2002) The Mre11 complex: at the crossroads of DNA repair and checkpoint signalling. *Nature Rev. Mol. Cell. Biol.*, **3**, 317–327.
10. Hopfner,K.P., Karcher,A., Craig,L., Woo,T.T., Carney,J.P. and Tainer,J.A. (2001) Structural biochemistry and interaction architecture of

the DNA double-strand break repair Mre11 nuclease and Rad50-ATPase. *Cell*, **105**, 473–485.
11. Bressan,D.A., Olivares,H.A., Nelms,B.E. and Petrini,J.H. (1998) Alteration of N-terminal phosphoesterase signature motifs inactivates *Saccharomyces cerevisiae* Mre11. *Genetics*, **150**, 591–600.
12. Paull,T.T. and Gellert,M. (1998) The 3′ to 5′ exonuclease activity of Mre 11 facilitates repair of DNA double-strand breaks. *Mol. Cell*, **1**, 969–979.
13. Paull,T.T. and Gellert,M. (1999) Nbs1 potentiates ATP-driven DNA unwinding and endonuclease cleavage by the Mre11/Rad50 complex. *Genes Dev.*, **13**, 1276–1288.
14. Usui,T., Ohta,T., Oshiumi,H., Tomizawa,J., Ogawa,H. and Ogawa,T. (1998) Complex formation and functional versatility of Mre11 of budding yeast in recombination. *Cell*, **95**, 705–716.
15. Connelly,J.C., Kirkham,L.A. and Leach,D.R. (1998) The SbcCD nuclease of *Escherichia coli* is a structural maintenance of chromosomes (SMC) family protein that cleaves hairpin DNA. *Proc. Natl Acad. Sci. USA*, **95**, 7969–7974.
16. Paull,T.T. and Gellert,M. (2000) A mechanistic basis for Mre11-directed DNA joining at microhomologies. *Proc. Natl Acad. Sci. USA*, **97**, 6409–6414.
17. Lobachev,K.S., Gordenin,D.A. and Resnick,M.A. (2002) The Mre11 complex is required for repair of hairpin-capped double-strand breaks and prevention of chromosome rearrangements. *Cell*, **108**, 183–193.
18. Richard,G.F., Goellner,G.M., McMurray,C.T. and Haber,J.E. (2000) Recombination-induced CAG trinucleotide repeat expansions in yeast involve the MRE11–RAD50–XRS2 complex. *EMBO J.*, **19**, 2381–2390.
19. Symington,L.S., Kang,L.E. and Moreau,S. (2000) Alteration of gene conversion tract length and associated crossing over during plasmid gap repair in nuclease-deficient strains of *Saccharomyces cerevisiae*. *Nucleic Acids Res.*, **28**, 4649–4656.
20. Serrano,M., Lin,A.W., McCurrach,M.E., Beach,D. and Lowe,S.W. (1997) Oncogenic ras provokes premature cell senescence associated with accumulation of p53 and p16INK4a. *Cell*, **88**, 593–602.
21. Brünger,A.T., Adams,P.D., Clore,G.M., DeLano,W.L., Gros,P., Grosse-Kunstleve,R.W., Jiang,J.S., Kuszewski,J., Nilges,M., Pannu,N.S. *et al*. (1998) Crystallography and NMR system: a new software suite for macromolecular structure determination. *Acta Crystallogr. D*, **54**, 905–921.
22. Stracker,T.H., Carson,C.T. and Weitzman,M.D. (2002) Adenovirus oncoproteins inactivate the Mre11–Rad50–NBS1 DNA repair complex. *Nature*, **418**, 348–352.
23. Paques,F. and Haber,J.E. (1999) Multiple pathways of recombination induced by double-strand breaks in *Saccharomyces cerevisiae*. *Microbiol. Mol. Biol. Rev.*, **63**, 349–404.
24. Griffith,J.P., Kim,J.L., Kim,E.E., Sintchak,M.D., Thomson,J.A., Fitzgibbon,M.J., Fleming,M.A., Caron,P.R., Hsiao,K. and Navia,M.A. (1995) X-ray structure of calcineurin inhibited by the immunophilin–immunosuppressant FKBP12–FK506 complex. *Cell*, **82**, 507–522.
25. Moreau,S., Ferguson,J.R. and Symington,L. (1999) The nuclease activity of Mre11 is required for meiosis but not mating type switching, end joining, or telomere maintenance. *Mol. Cell. Biol.*, **19**, 556–566.
26. Uziel,T., Lerenthal,Y., Moyal,L., Andegeko,Y., Mittelman,L. and Shiloh,Y. (2003) Requirement of the MRN complex for ATM activation by DNA damage. *EMBO J.*, **22**, 5612–5621.
27. Carson,C.T., Schwartz,R.A., Stracker,T.H., Lilley,C.E., Lee,D.V. and Weitzman,M.D. (2003) The Mre11 complex is required for ATM activation and the G(2)/M checkpoint. *EMBO J.*, **22**, 6610–6620.